Supporting Information

Dynamic Stabilization of Nickel-based Oxygen Evolution Electrocatalysts in the Presence of Chloride Ions by Phosphate Additive

Hiroki Komiya, Keisuke Obata, Tetsuo Honma, Kazuhiro Takanabe*

Table of Contents

1. Results and Discussion

1.1 The role of phosphate on the oxygen evolution reaction

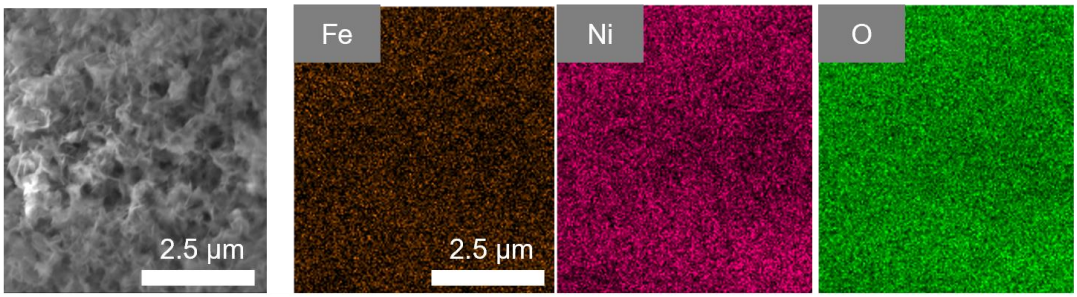

Fig. S1. Scanning electron microscope (SEM) and energy dispersive X-ray spectroscopy (EDS) images of as made $NiFeO_x$/NF.

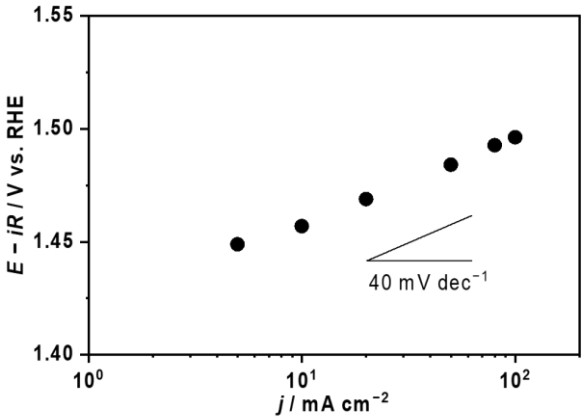

Fig. S2. Tafel slope analysis over $NiFeO_x$/Ni foam (NF) synthesized by hydrothermal method. Tafel plots at steady state were obtained from chronopotentiometry (CP). CP was conducted in 1 mol L^{-1} KOH solution at pH 14 at 298 K.

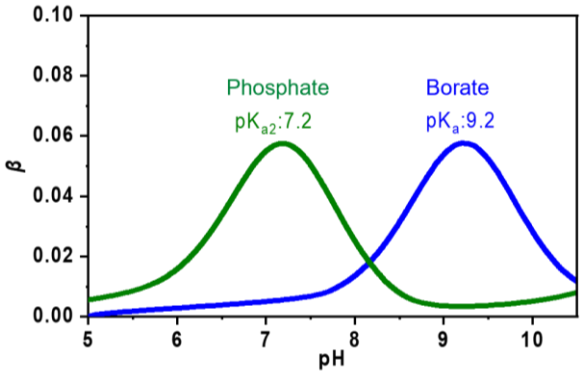

Fig. S3. The illustration of buffer capacity (*β*) as a function of pH. The concentration of borate and phosphate was fixed at 0.1 mol L^{-1}. The simulation curve was calculated by HySS software based on the solution pK_a values.

Buffer capacity (*β*) is calculated based on how pH changes when the acid or base is introduced into the system as expressed in **Equation (1)**.

$$\beta = \frac{d[OH^-]}{d(pH)} = \frac{d[A^-]}{d(pH)} \qquad (1)$$

$[OH^-]$ is the concentration of added base, and $[A^-]$ is the concentration of buffer substance. This buffer capacity shows a maximum value at pH closer to its intrinsic pK_a as illustrated in **Fig. S3. Fig. S3** depicts the buffer capacity as a function of solution pH. Both borate and phosphate concentrations were fixed at 0.1 mol L^{-1}. The intensity is maximum at pH 7.2 for phosphate and 9.2 for borate, which corresponds with the intrinsic pK_a of buffer species (phosphate: pK_{a2}=7.2, borate: pK_a=9.2). As a result, when we employed the solution at pH 9.2 and the same concentration, the borate electrolyte showed a lower concentration overpotential due to higher buffer capacity than phosphate to maintain the local pH shifting at that pH (see **Fig. 1a**).

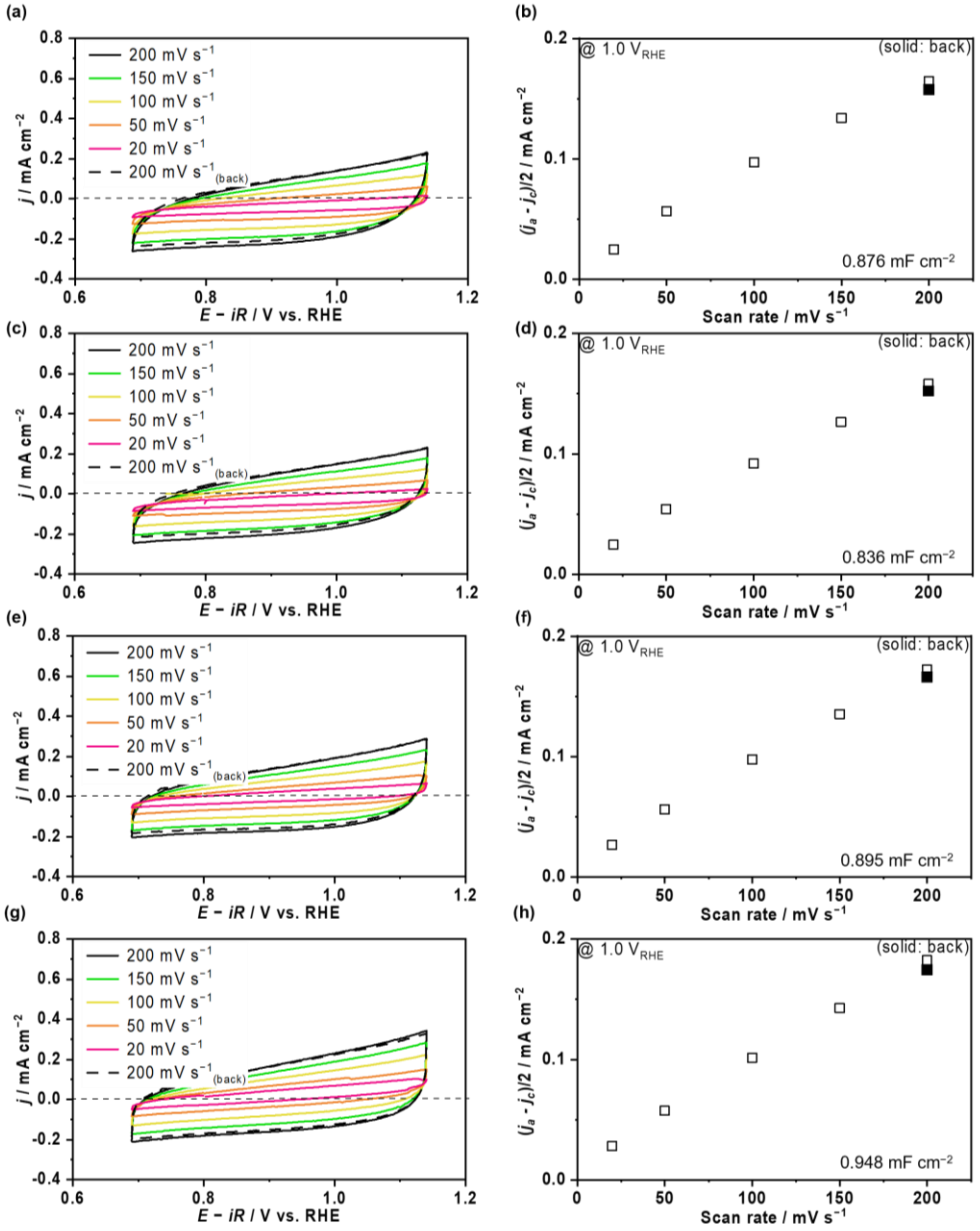

Fig. S4. Double-layer capacitance (C_{dl}) analysis over $NiFeO_x$/Ni foam in various mixed buffer electrolytes after OER testing. Cyclic voltammograms (CV) profiles and currents density (j) at suitable potential specified at the left-hand corner of the figure vs. RHE as a function of scan rate were recorded in (a)(b) 1.0 mol kg^{-1} K-borate, (c)(d) 1.0 mol kg^{-1} K-borate + 0.5 mol kg^{-1} K-phosphate, (e)(f) 1.0 mol kg^{-1} K-borate + 1.0 mol kg^{-1} K-phosphate, (g)(h) 1.0 mol kg^{-1} K-borate + 2.0 mol kg^{-1} K-phosphate electrolyte at pH 9.2 and 298 K with Ar bubbling.

We examined the double-layer capacitance (C_{dl}) which reflects the electrochemically active surface area over $NiFeO_x$/Ni foam in various electrolytes (borate, borate/phosphate) by employing the cyclic voltammogram (see **Fig. S4**). The C_{dl} is the slope value of the scan rate versus the average of anodic and cathodic current densities (j_a and j_c are anodic and cathodic current densities). The capacitance values in the right corner were almost constant among various electrolyte conditions, indicating the negligible loss of electrochemically active surface area by phosphate additives.

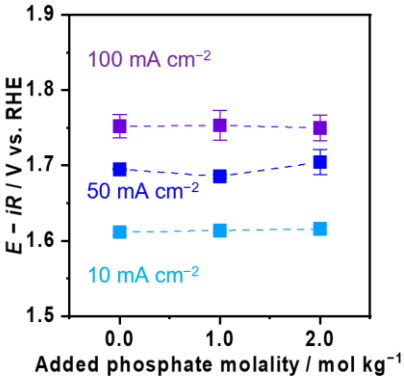

Fig. S5. OER potentials over $NiFeO_x$/NF in dense K-borate electrolyte with phosphate additives. The potentials at each current density were recorded using the steady state CP in 1.5 mol kg^{-1} K-borate + various molality of K-phosphate with O_2 bubbling at pH 9.2 and 298 K.

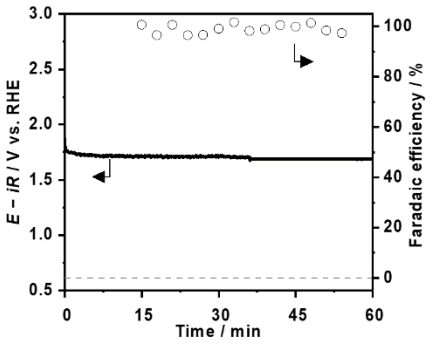

Fig. S6. Faradaic efficiency measurement over $NiFeO_x$/NF in K-borate/phosphate electrolyte at room temperature. The potential profile was recorded using the CP at 50 mA cm^{-2} in 1.0 mol kg^{-1} K-borate + 1.0 mol kg^{-1} K-phosphate electrolytes at pH 9.2. Faradaic efficiency (FE) of O_2 (FE_{O2}) was calculated based on the amount of generated gas detected by the gas chromatography.

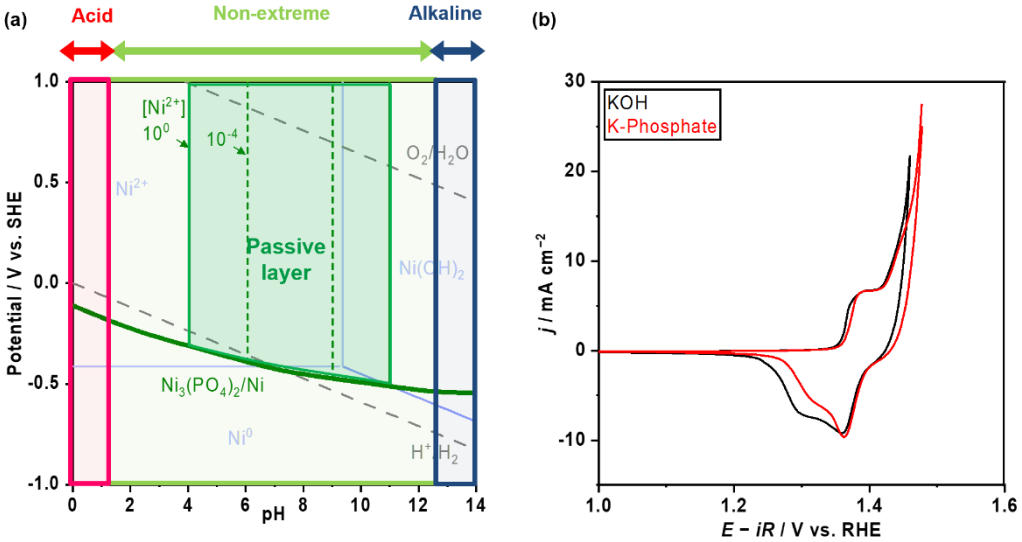

Fig. S7. Investigation of the thermodynamical stability of Ni-passive layer. (a) Pourbaix diagram of Ni in the presence of phosphate anion. The lines were calculated based on the thermodynamic properties of each product (Table S1). The unit of $[Ni^{2+}]$ is mol L^{-1}. (b) Cyclic voltammetry (CV) profiles over $NiFeO_x$/NF in KOH and K-phosphate at pH 14 and 298 K. CVs were recorded at a scan rate of 1 mV s^{-1}.

Table S1. Thermodynamic properties of products.

	Thermodynamic data[1]		
	State	ΔG_f / kJ mol^{-1}	a or f / mol L^{-1}
Ni	cr	0	1
Ni^{2+}	a_0	−45.6	10^{-6}
$Ni(OH)_2$	cr	−447.2	1
$Ni_3(PO_4)_2$	cr	−2353	1
$H_2PO_4^-$	a_0	−1130.28	-
PO_4^{3-}	a_0	−1018.7	-
H^+	a_0	0	-
OH^-	a_0	−157.244	-
H_2O	l	−237.129	1

Physical states: cr is the crystalline solid state. l is the liquid state. a_0 is the aqueous solution, an un-ionized substance, standard state at 1 mol kg^{-1}.

The concertation of phosphate varies with pH. So, the molar fraction of species was calculated based on its intrinsic pK_a value. Phosphate: pK_{a1}=2.1, pK_{a2}=7.2, pK_{a3}=12.7. The concentration of phosphate was fixed at 1.0 mol L^{-1} unless otherwise specified.

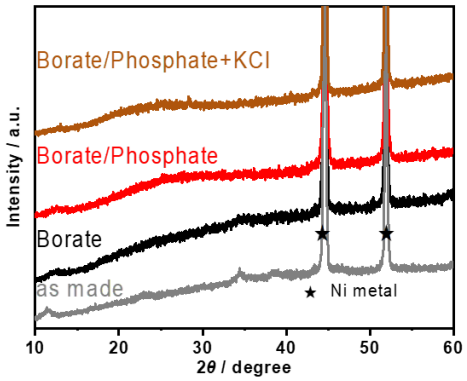

Fig. S8. X-ray diffraction patterns of as made and post OER $NiFeO_x$/NF. OER measurements were conducted in 1.0 mol kg^{-1} K-borate, 1.0 mol kg^{-1} K-borate + 1.0 mol kg^{-1} K-phosphate, and 1.0 mol kg^{-1} K-borate + 1.0 mol kg^{-1} K-phosphate + 0.5 mol kg^{-1} KCl at pH 9.2, 298 K.

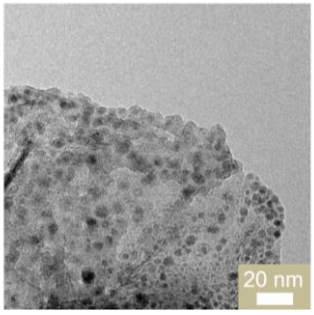

Fig. S9. Transmission electron microscopy (TEM) image of post-reacted $NiFeO_x$. The OER testing was conducted in the K-borate/phosohate (1.0 mol kg^{-1} K-borate + 1.0 mol kg^{-1} K-phosphate) electrolyte at room temperature and pH 9.2.

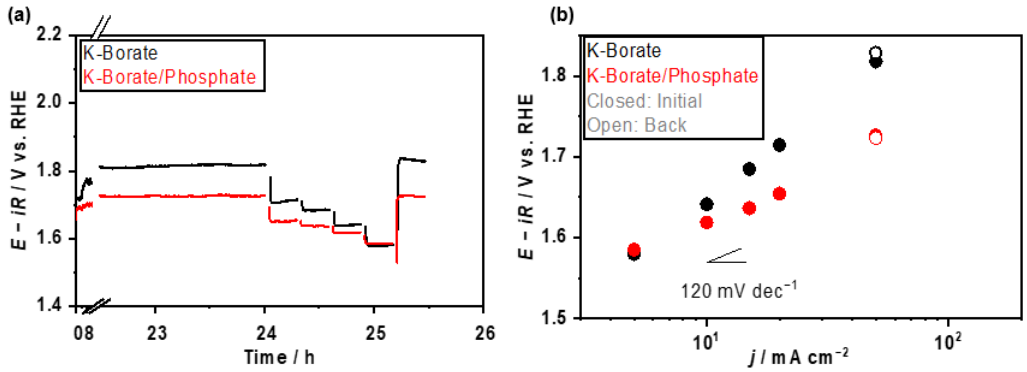

Fig. S10. Stability testing and stepwise CP profile over $NiFeO_x$/Ni foam with and without phosphate additives at room temperature. (a) Potential profiles over $NiFeO_x$/Ni foam in 1.5 mol kg^{-1} K-borate (black) and 1.0 mol kg^{-1} K-borate + 2.0 mol kg^{-1} K-phosphate (red) at pH 9.2. The potential profiles were recorded using CP at 50 mA cm^{-2} for 24 h. After that, the current density decreased 20, 15, 10, 5 mA cm^{-2} for 15 min each. Finally, the current density went back to the original value of 50 mA cm^{-2}. (b) CVs over $NiFeO_x$/Ni foam were recorded at a scan rate of 1 mV s^{-1} after the stability testing. All electrolytes were saturated with O_2 during measurements.

The acquired CV contains the oxidation of the electrode and does not precisely reflect the oxygen evolution reaction; thus, OER performance looks like to be improved as shown in **Fig. 3b**. To accurately evaluate the required potentials for OER, we intentionally change the current density stepwise after stability testing as shown in **Fig. S10a**. In detail, newly conducted stability testing proceeded at 50 mA cm^{-2} for 24 h, and then the current density was decreased to 20, 15, 10, and 5 mA cm^{-2} for 15 min each. Finally, the current density was switched back to the original value of 50 mA cm^{-2}. The Tafel slope (**Fig. S10b**) plotted based on the steady-state CP shows that the required potentials at 50, 20, 15, 10, and 50 (back) mA cm^{-2} were smaller in the borate/phosphate solution than in the borate one and the slope value was smaller than that in borate likely due to the small electrode composition change due to suppressed dissolution of Ni. This result supports the degradation of electrodes in borate electrolytes. Thus, the required potential increment at 50 mA cm^{-2} during the stability testing is convincing to assess the degradation of electrodes. We would like to emphasize that our intention to obtain CVs in **Fig. 3b** was to investigate the reduction peak of $Ni^{2+/3+}$ species and that OER activity should be evaluated by steady-state CPs

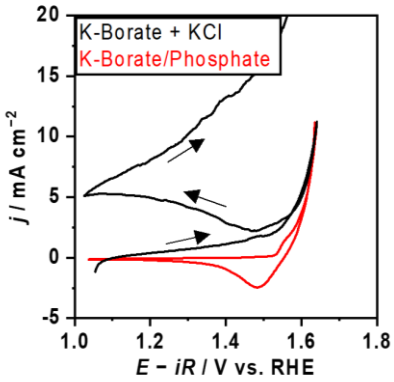

Fig. S11. Electrolyte replacement test over $NiFeO_x$/NF. CV was recorded after OER measurements in K-borate/phosphate electrolyte (red), and then the $NiFeO_x$ electrode was immersed in K-borate with KCl electrolyte, and CV was recorded (black). The molality of K-borate was 1.0 mol kg^{-1}, that of K-borate/phosphate was 1.0 mol kg^{-1} K-borate + 1.0 mol kg^{-1} phosphate, and that of KCl was 0.5 mol kg^{-1}. OER measurements were conducted with O_2 bubbling and at pH 9.2.

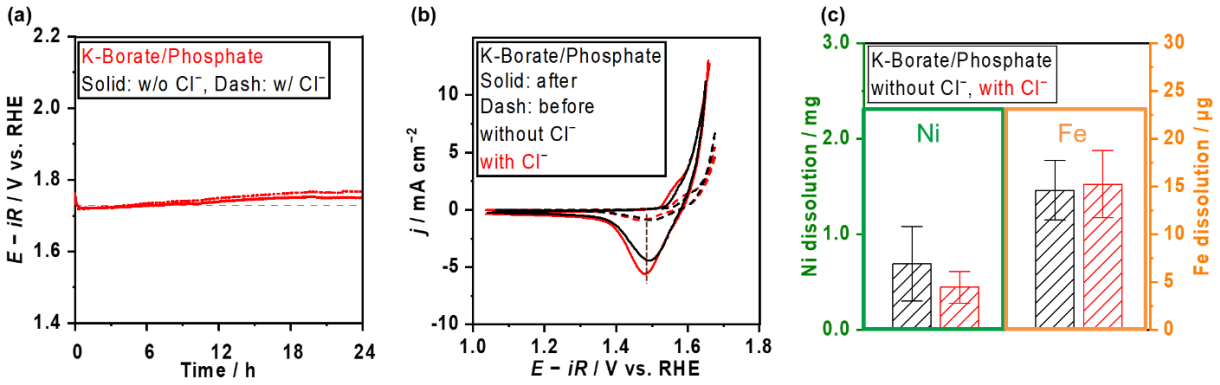

Fig. S12. Stability testing over $NiFeO_x$/NF in mixed buffer electrolyte with the existence of Cl^-. (a) Potential profiles at 50 mA cm^{-2} in 1.0 mol kg^{-1} K-borate + 1.0 mol kg^{-1} K-phosphate with and without 0.5 mol kg^{-1} KCl at pH 9.2 and 298 K. (b) CV before and after stability testing. CVs were recorded at a scan rate of 1 mV s^{-1}. All electrolytes were saturated with O_2 during the test. (c) Metal dissolution amount of Ni and Fe in electrolytes after stability testing.

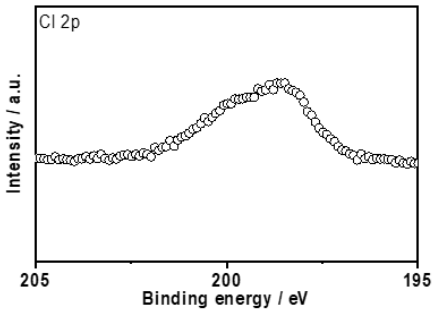

Fig. S13. Xay photoelectron spectroscopy (XPS) spectra of the Cl 2p over $NiFeO_x$/Ni felt after OER testing in 1.0 mol kg^{-1} K-borate + 1.0 mol kg^{-1} K-phosphate + 0.5 mol kg^{-1} KCl electrolyte. The OER measurements were conducted with O_2 bubbling at 298 K, pH 9.2.

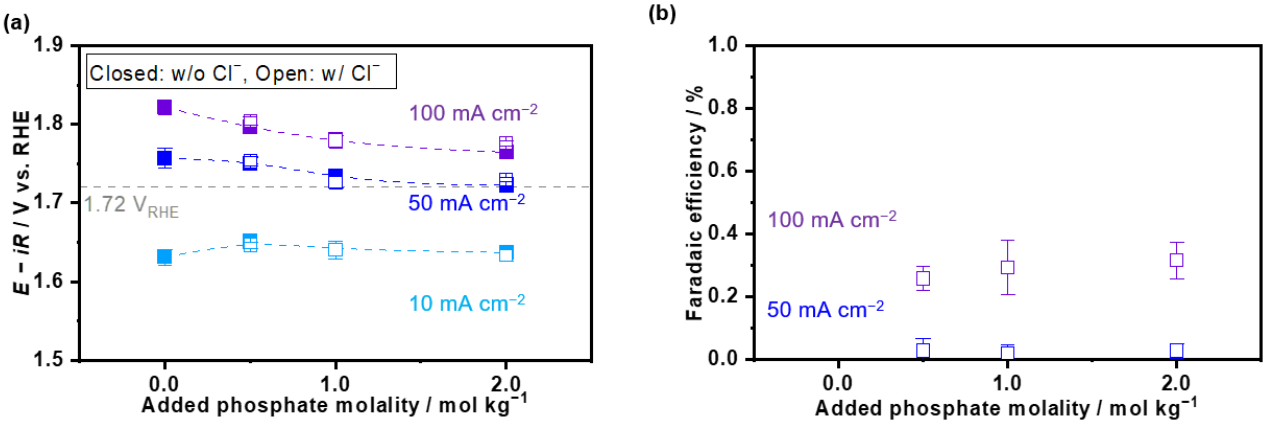

Fig. S14. OER performance over $NiFeO_x$/NF in mixed buffer electrolytes in the presence of Cl^-. (a) Potential at different *j* as a function of added phosphate molality. The molality of K-borate and KCl were fixed at 1.0 mol kg^{-1} and 0.5 mol kg^{-1}, respectively. Potentials were recorded by using the steady state CP. (b) Faradaic efficiency (FE) of hypochlorite (ClO^-) formation reaction (FE_{HC}) at different current densities. FE_{HC} was calculated based on the remained ClO^- amount in electrolytes after time-controlled CP. The amount of ClO^- was qualified using the calibration made by utilizing the DPD method. All electrolytes were saturated with O_2 during measurements and fixed at pH 9.2 and 298 K.

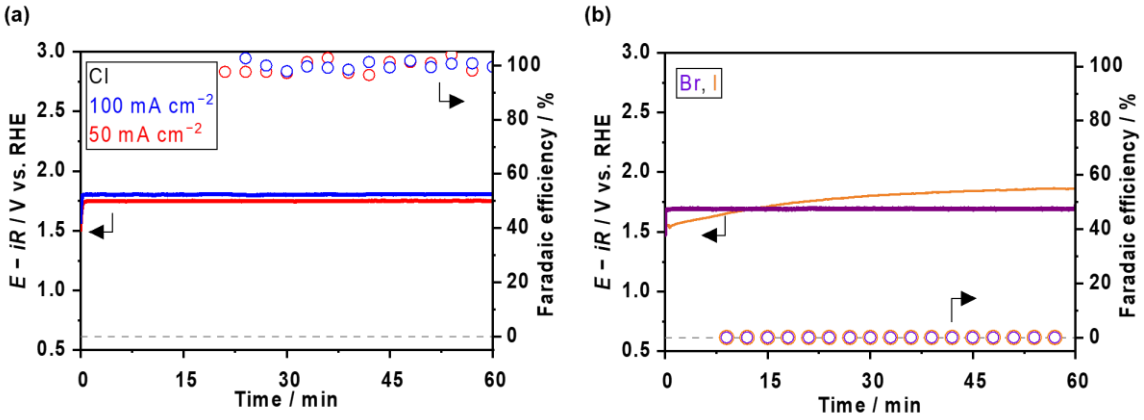

Fig. S15. Potential profiles over $NiFeO_x$/NF during the FE measurements in mixed buffer electrolytes in the presence of halide ions. Potentials and FE_{O2} at different current densities versus time in 1.0 mol kg^{-1} K-borate + 1.0 mol kg^{-1} K-phosphate at pH 9.2 and 298 K containing 0.5 mol kg^{-1} of (a) KCl, (b) KBr and KI. The applied current density was 50 mA cm^{-2} unless otherwise specified in the figure. FE_{O2} values were calculated based on generated gas detected by gas chromatography.

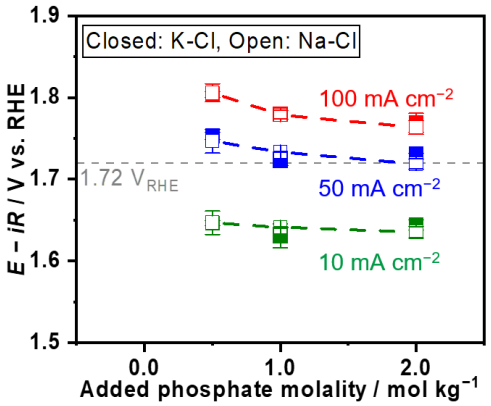

Fig. S16. OER performance over $NiFeO_x$/NF in mixed buffer electrolytes in the presence of K and Na-Cl. Potential at different *j* as a function of added phosphate molality. The molality of K-borate and Na/K-Cl were fixed at 1.0 mol kg^{-1} and 0.5 mol kg^{-1}, respectively. Potentials were recorded by using the steady-state CP. All electrolytes were saturated with O_2 during measurements and fixed at pH 9.2 and 298 K.

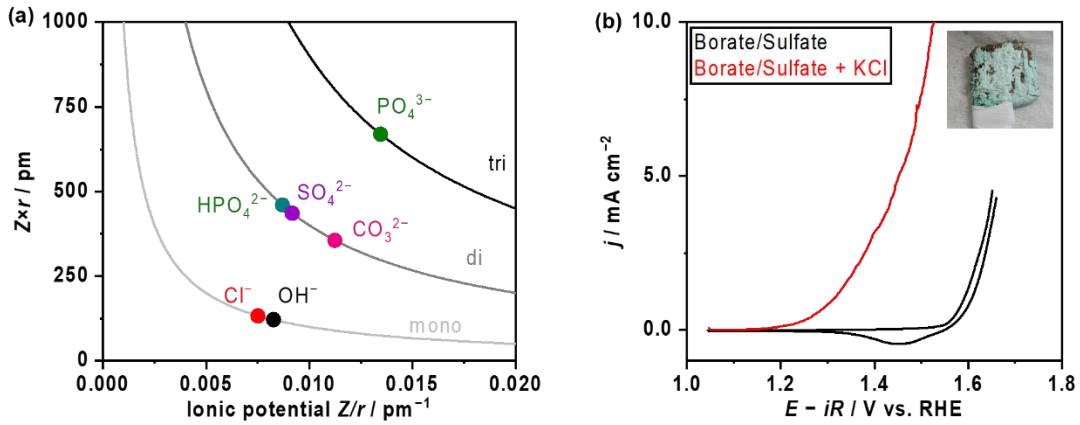

Fig. S17. Charge repulsion capacity and its application for stabilizing $NiFeO_x$ electrode. (a) Charge repulsion capacity diagram. X-axis and Y-axis show the ionic potential calculated by dividing ion charge (*Z*) by stokes radius (*r*) and *Z*×*r*, respectively. (b) CV profile over $NiFeO_x$/NF in 1.0 mol kg^{-1} K-borate + 0.5 mol kg^{-1} K-sulfate with and without 0.5 mol kg^{-1} KCl at pH 9.2, 298 K. The scan rate was 1 mV s^{-1}. The photo was post-reacted $NiFeO_x$/NF in the presence of Cl^-.

1.2 The oxidations of various redox probes over $NiFeO_x$/NF.

Alcohols

The OER performance was also assessed in the alcohol-containing electrolytes. **Fig. S18a and b** illustrate the redox feature of $NiFeO_x$ in the presence of EtOH at pH 9.2 and 11. pH 11 was selected as a more alkaline condition to find the pH dependence of the EtOH oxidation reaction (EOR), where the dominant phosphate charge is maintained at −2. The Ni reduction potential peak shifted to more positive by adding phosphate irrespective of bulk pH level, indicating the formation of Ni phosphate complex. **Fig. S18c** shows the FE_{O2} at different pH levels. Interestingly, the FE_{O2} increased with the introduced phosphate into the electrolytes at both pH levels. **Fig. S18d** compares the Tafel slope in two kinds of pH levels below diffusion limited *j* for EOR (ca. 10 mA cm^{-2}).[2] At pH 9.2 and 11, the slope values were dissimilar for with and without phosphate, indicating that the reaction kinetic is altered by adding phosphate. Together with the result of the FE and Tafel slope value, the role of the phosphate is estimated to switch the active site from Ni to Fe by forming a Ni-based passive layer. Because Fe hydroxide is not a superior catalyst for EOR than Ni hydroxide,[3] active site switching allowed the $NiFeO_x$ to produce more O_2. In addition, **Fig. S18e and f** show the potential profiles during the FE measurements, which are conducted through chronopotentiometry (CP) at 50 mA cm^{-2} and 298 K. At pH 9.2, the potential increased in the single borate system; however, the potential was stable in a borate/phosphate mixed buffer system. This is because the EOR accompanies the formation of the AcOH, which alters the local pH to more acidic, leading to the thermodynamic corrosion of the Ni hydroxide. At pH 11, the potential was stable due to the abundant base to replenish the formed acid. O_2 selectivity at pH 9.2 was better than alkaline counterparts due to the pH dependence of EOR.[4] The *i*-PrOH oxidation reaction was also examined. **Fig. S19** shows the CVs and FE_{O2} in two different buffer electrolytes with *i*-PrOH. Although the redox feature was like the EtOH case, there was no significant FE improvement, indicating the *i*-PrOH oxidation would mostly likely proceed with the Fe site, and the tiny difference of FE between with and without phosphate condition can be attributed to the diffusion rate of the *i*-PrOH, which is determined by the electrolyte viscosity induced by the addition of the phosphate.

Other negatively charged probes

As discussed in the main text, the $[Fe(CN)_6]^{4-}$ was oxidized even in the presence of the phosphate additive. This highlights that the main role of the phosphate is to stabilize the Ni rather than charge the repulsion effect. The slight difference in the FE_{O2} can be attributed to the difference in the diffusion rate of the $[Fe(CN)_6]^{4-}$. **Fig. S21a and b** show the CVs and FE with and without formate. Formate is easily oxidized into the CO_2 through the two-electron transfer.[5] From the result of the FE, almost all the electrons were used to oxidize the formate to CO_2. "×" shown in **Fig. 21b** means failure to acquire FE due to the high corrosiveness of the $NiFeO_x$/NF in a single borate electrolyte. In contrast, the potential profile in the presence of phosphate was stable (**Fig. S21c**).

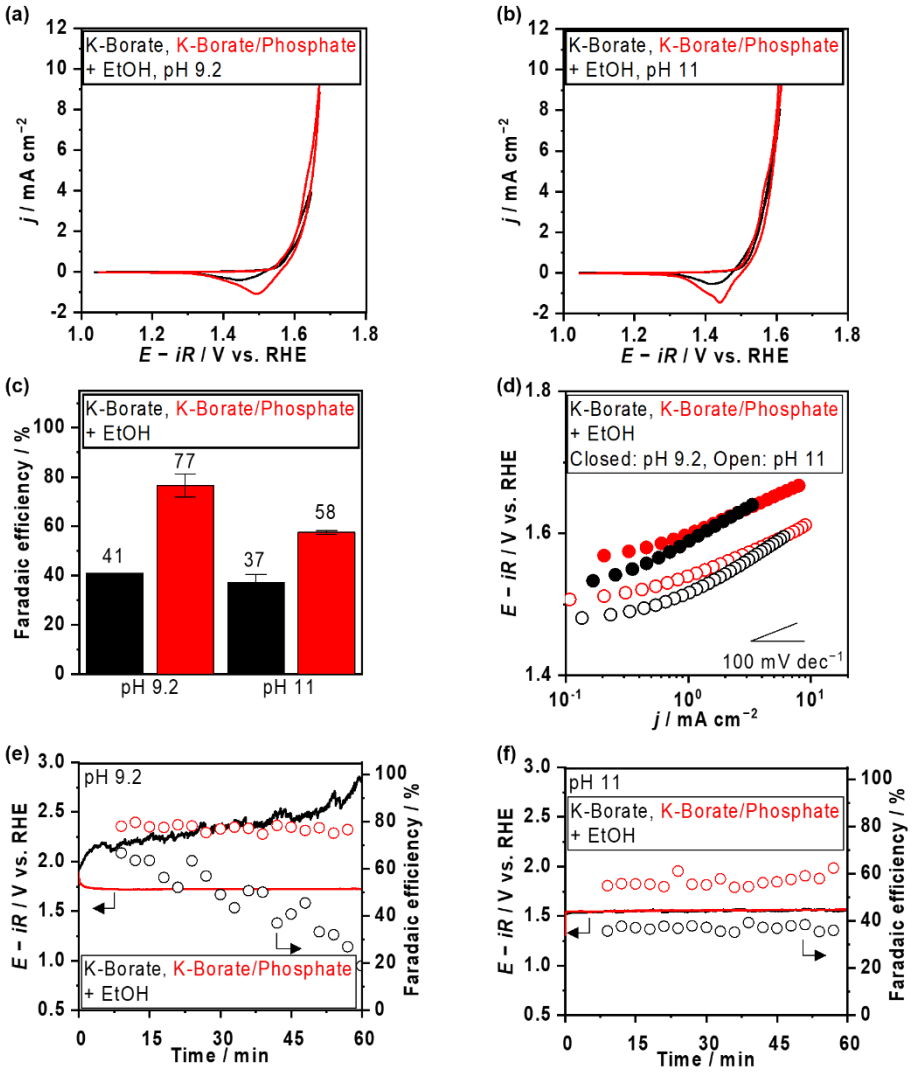

Fig. S18. OER performance over $NiFeO_x$ in EtOH-containing electrolytes at room temperature. CV profiles in K-borate and K-borate/phosphate electrolytes with EtOH at pH (a) 9.2, (b) 11. The molality of K-borate was 1.0 mol kg^{-1}, of K-borate/phosphate was 1.0 mol kg^{-1} K-borate + 1.0 mol kg^{-1} phosphate, and of EtOH was 0.4 mol kg^{-1}. (c) The trend of FE_{O2} in various electrolytes with EtOH. The FE measurement was conducted by utilizing the CP technique at 50 mA cm^{-2}, and the FE values were calculated based on generated gas detected on gas chromatography. (d) *j* versus potential profiles in various electrolytes in the presence of EtOH additives. (e) (f) Potential and FE_{O2} profiles over $NiFeO_x$ during FE measurements at 50 mA cm^{-2} in K-borate and K-borate/phosphate electrolytes at pH (e) 9.2, (f) 11.0. The molality of K-borate was 1.0 mol kg^{-1}, of K-borate/phosphate was 1.0 mol kg^{-1} K-borate + 1.0 mol kg^{-1} phosphate, and of EtOH was 0.4 mol kg^{-1}. FE values were calculated based on the generated gas detected by gas chromatography.

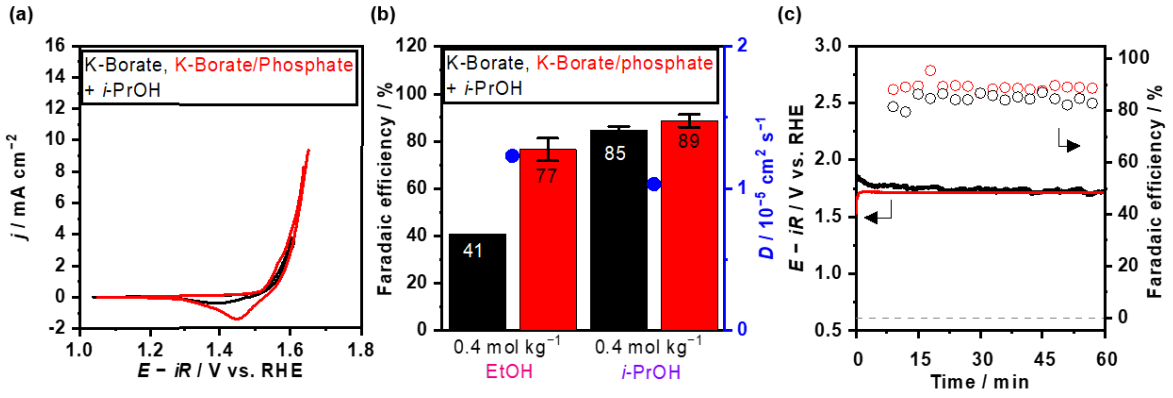

Fig. S19. OER performance over $NiFeO_x$/NF in the presence of *i*-PrOH at room temperature. (a) CV profiles, (b) FE_{O2}, and (c) potential and FE_{O2} profiles during FE measurement in 1.0 mol kg^{-1} K-borate and 1.0 mol kg^{-1} K-borate + 1.0 mol kg^{-1} K-phosphate, both of which contain 0.4 mol kg^{-1} *i*-PrOH and were fixed at pH 9.2. CVs were recorded at a scan rate of 1 mv s^{-1}. FE_{O2} measurement was conducted using CP at 50 mA cm^{-2} for 1 h. FE_{O2} was calculated based on the generated gas detected by gas chromatography.

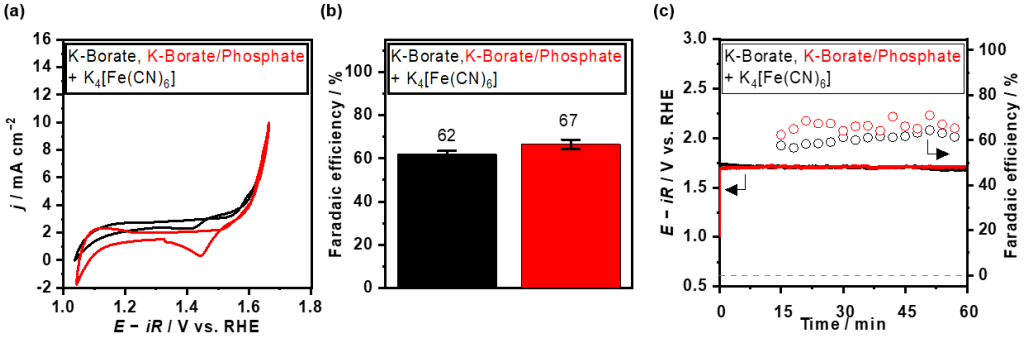

Fig. S20. OER performance over $NiFeO_x$/NF in the presence of $K_4[Fe(CN)_6]$ at room temperature. (a) CV profiles, (b) FE_{O2}, and (c) potential and FE_{O2} profiles during FE measurement in 1.0 mol kg^{-1} K-borate and 1.0 mol kg^{-1} K-borate + 1.0 mol kg^{-1} K-phosphate, both of which contain 0.1 mol kg^{-1} $K_4[Fe(CN)_6]$ and were fixed at pH 9.2. CVs were recorded at a scan rate of 1 mv s^{-1}. FE_{O2} measurement was conducted using CP at 50 mA cm^{-2} for 1 h. FE_{O2} was calculated based on the generated gas detected by gas chromatography.

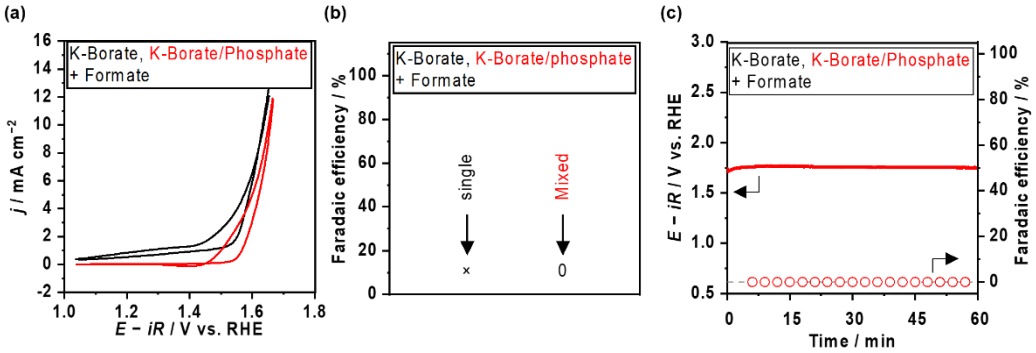

Fig. S21. OER performance over $NiFeO_x$/NF in the presence of formate at room temperature. (a) CV profiles, (b) FE_{O2}, and (c) potential and FE_{O2} profiles during FE measurement in 1.0 mol kg^{-1} K-borate and 1.0 mol kg^{-1} K-borate + 1.0 mol kg^{-1} K-phosphate, both of which contained 0.4 mol kg^{-1} formate and were fixed at pH 9.2. CVs were recorded at a scan rate of 1 mv s^{-1}. FE_{O2} measurement was conducted using CP at 50 mA cm^{-2} for 1 h. FE_{O2} was calculated based on the generated gas detected by gas chromatography.

1.3 OER experiments at elevated temperatures.

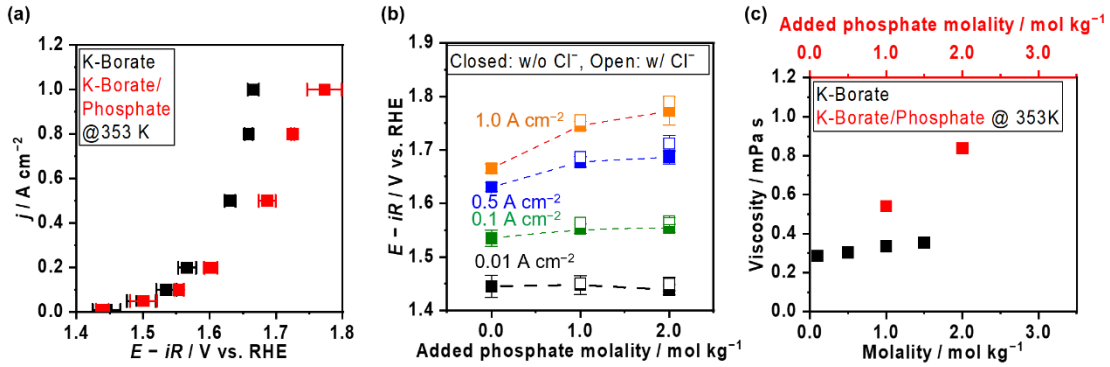

Fig. S22. Evaluation of OER performance over $NiFeO_x$/NF at elevated temperature at pH 9.2. (a) Potential and *j* relationship in single 1.5 mol kg^{-1} K-borate and 1.5 mol kg^{-1} K-borate + 2.0 mol kg^{-1} K-phosphate mixed buffer electrolyte at 353 K. (b) Potentials at different *j* versus molality of added phosphate ion at 353 K with chloride ions. All potentials were recorded by using the steady-state CP. The molalities of borate and KCl were fixed at 1.5 mol kg^{-1} and 0.5 mol kg^{-1}, respectively. (c) Electrolytes viscosity at 353 K. Black plots correspond with single K-borate. Red plots correspond with the viscosity, including the different molality of phosphate in K-borate, whose molality was fixed at 1.5 mol kg^{-1}. All OER measurements were conducted with O_2 bubbling.

1.4 XAS experiments

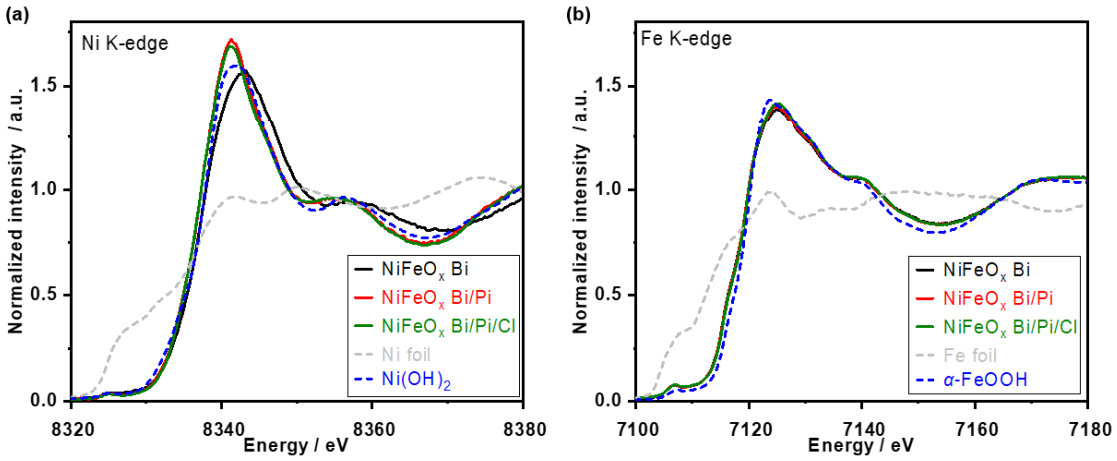

Fig. S23. Ex-situ X-ray absorption spectroscopy (XAS) analysis over $NiFeO_x$ catalysts. X-ray absorption near edge structure (XANES) spectra of (a) Ni K-edge, (b) Fe K-edge. Ex-situ means that the catalysts were activated through the 1h CP at 10 mA cm^{-2} in 1.0 mol kg^{-1} K-borate (Bi), 1.0 mol kg^{-1} K-borate + 1.0 mol kg^{-1} K-phosphate (Bi/Pi), 1.0 mol kg^{-1} K-borate + 1.0 mol kg^{-1} K-phosphate + 0.5 mol kg^{-1} K-Cl (Bi/Pi/Cl) at pH 9.2 and 298 K.

1.5 Other experiments

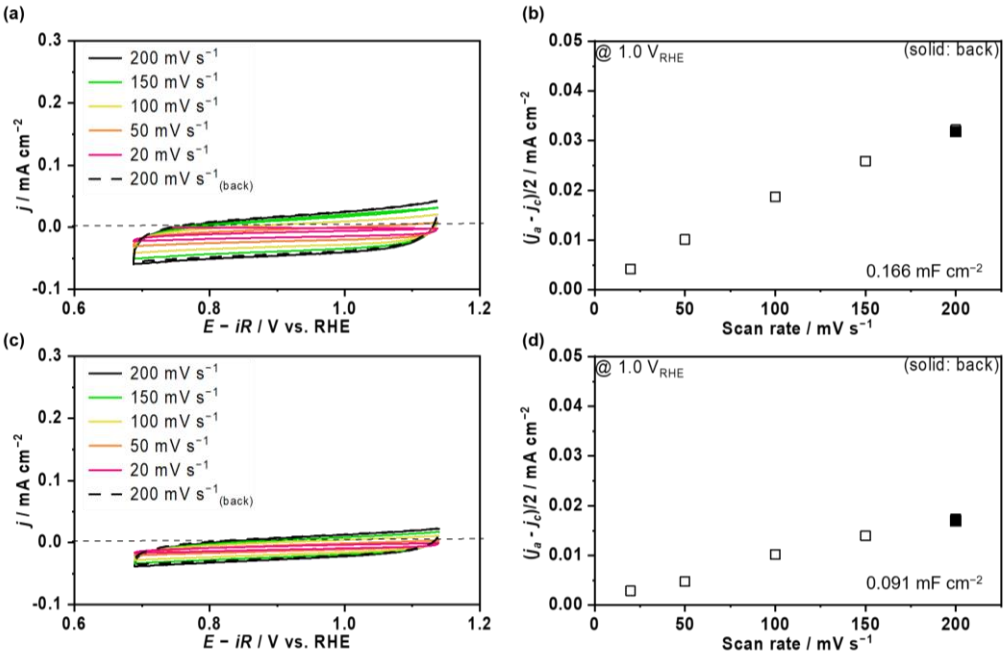

Fig. S24. Double-layer capacitance (C_{dl}) analysis over $NiFeO_x$/Ni felt and $NiFeO_x$/Ni plate after OER testing. CV profiles and *j* at suitable potential specified at the left-hand corner of the figure vs. RHE as a function of scan rate were recorded over (a)(b) $NiFeO_x$/Ni felt, (c)(d) $NiFeO_x$/Ni plate in 1.0 mol kg^{-1} K-borate at pH 9.2 and 298 K with Ar bubbling.

2. References

1 D. D. Wagman, *The NBS tables of chemical thermodynamic properties: Selected values for inorganic and C1 and C2 organic substances in SI units*, American Chemical Society, New York, N.Y;Washington, D.C;, 1982.
2 E. E. Hills, M. H. Abraham, A. Hersey and C. D. Bevan, *Fluid Phase Equilibria*, 2011, **303**, 45–55.
3 D. Martín-Yerga, G. Henriksson and A. Cornell, *Electrocatalysis*, 2019, **10**, 489–498.
4 S. C. S. Lai, S. E. F. Kleijn, F. T. Z. Öztürk, V. C. van Rees Vellinga, J. Koning, P. Rodriguez and M. T. M. Koper, *Catal. Today*, 2010, **154**, 92–104.
5 Y. Cao, Q. Chen, C. Shen and L. He, *Mol. Basel Switz.*, 2019, **24**, 2069.